



Original article

Synthesis, biological evaluation and molecular modeling of 4,6-diarylpyrimidines and diarylbenzenes as novel non-nucleosides HIV-1 reverse transcriptase inhibitors

Sergio R. Ribone^a, Volker Leen^b, Marcela Madrid^c, Wim Dehaen^b, Dirk Daelemans^d, Christophe Pannecouque^{d,**}, Margarita C. Briñón^{a,*}

^a Departamento de Farmacia, Facultad de Ciencias Químicas, Ciudad Universitaria, Universidad Nacional de Córdoba, X5000HUA Córdoba, Argentina

^b Pittsburgh Supercomputing Center, Pittsburgh, PA 15213, USA

^c Chemistry Department, KU Leuven, Celestijnenlaan 200F, 3001 Leuven, Belgium

^d Rega Institute for Medical Research, KU Leuven, Minderbroedersstraat 10, B-3000 Leuven, Belgium

ARTICLE INFO

Article history:

Received 21 September 2012

Received in revised form

15 October 2012

Accepted 20 October 2012

Available online 29 October 2012

Keywords:

HIV-1

NNRTIs

4,6-Diarylpyrimidines

Diarylbenzenes

Molecular modeling

SAR

ABSTRACT

A series of novel 4,6-diarylpyrimidines (4,6-DAPY) and diarylbenzenes (DABE) compounds were synthesized and evaluated as inhibitors of human immunodeficiency virus type-1 (HIV-1). Among them, the most potent HIV-1 inhibitors were **8b**, **8d**, **14b** and **18** (EC_{50} = 0.049, 0.381, 0.599 and 0.398 μ M, respectively), with HIV-1 inhibitory activity improved or similar to nevirapine (NVP, EC_{50} = 0.097 μ M) and delavirdine (DEV, EC_{50} = 0.55 μ M). The other compounds displayed moderate activity (**8c**, EC_{50} = 5.25 μ M) or were inactive (**8a** and **14a**) against HIV-1 replication. Molecular modeling studies were performed with the synthesized compounds in complex with the wild-type reverse transcriptase (RT). A correlation was found between the anti-HIV activity and the electrostatic energy of interaction with Lys101 residue. These findings enrich the SAR of these Non-Nucleoside Reverse Transcriptase Inhibitors (NNRTIs) families.

© 2012 Elsevier Masson SAS. All rights reserved.

1. Introduction

Human immunodeficiency virus (HIV) is the causative virus of acquired immunodeficiency syndrome (AIDS). At present, there is no effective vaccine against HIV, and the generally adopted highly active antiretroviral therapy (HAART) has significantly reduced the morbidity and mortality of HIV-infected people [1]. Reverse Transcriptase (RT) of the HIV-1, is an enzyme essential for the replication of the virus, and is one of the main targets for antiretroviral chemotherapy [2]. Non-Nucleoside Reverse Transcriptase Inhibitors (NNRTI), a class of components of HAART, elicit viral reverse transcription inhibition by binding to an allosteric pocket located 10 Å away from the DNA polymerase active site, the NNRTI Binding Pocket (NNIBP) [3,4].

Since their discovery, NNRTIs have received special attention due to their high antiviral activity and low cytotoxicity [5]. However, the rapid emergence of viral drug resistance prompted the development of diverse structures of NNRTI, such as 2-[(2-acetyl-5-methylphenyl)amino]-2-(2,6-dichlorophenyl)acetamide (α -APA) [6,7], benzophenones [8,9], dihydro-alkoxybenzyl-oxypyrimidines (DABOs) [10,11], diaryltriazines (DATAs) [12,13], and diarylpyrimidines (DAPYs) [14–16]. In particular, DAPYs have been regarded as one of the most successful scaffolds for NNRTIs because of their potent antiviral activity against wild-type and mutant strains of the HIV-1. Their molecular structure consists of three rings bound by rotatable bonds with a NH moiety linker between wing II and the central ring (Fig. 1) [3,4].

Because of their high antiviral potency, in previously published work, we carried out molecular modeling of DAPYs compounds and other different NNRTI, among them, those of first generation, in order to reveal the structural bases for the design of novel highly potent NNRTIs [17]. We concluded that a potent inhibitor of wild-type RT (wtRT) must possess the following structural properties: a) maximized van der Waals interactions in the NNIBP, b) hydrogen bond interaction with Lys101 residue and c) high molecular

Abbreviations: 4,6-DAPY, 4,6-diarylpyrimidines; DABE, diarylbenzenes.

* Corresponding author. Tel.: +54 0351 5353865x53355; fax: +54 0351 5353865x53364.

** Corresponding author. Tel.: +32 016 332171; fax: +32 016 332131.

E-mail addresses: christophe.pannecouque@rega.kuleuven.be (C. Pannecouque), macribri@fcq.unc.edu.ar (M.C. Briñón).

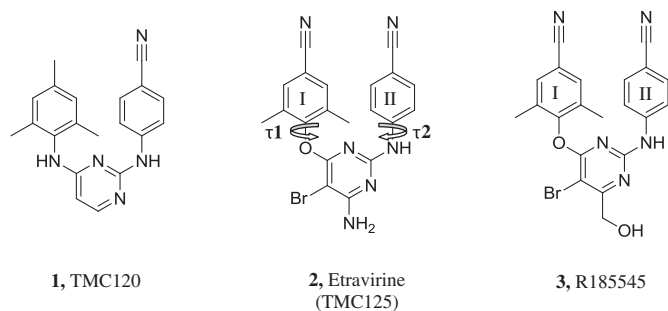


Fig. 1. Chemical structures of DAPYs compounds.

flexibility between the central ring and the lateral wings (Fig. 1, I and II in compounds **2** and **3**). Following these guidelines, we designed novel NNRTIs which kept the overall molecular structure of DAPYs, but incorporated 4,6-pyrimidine and benzene as central ring (Schemes 1–3).

The aim of the present work was to examine the influence of 4,6-pyrimidine and benzene as central rings, leading to novel structural scaffolds (4,6-diarylpyrimidines, 4,6-DAPYs and diarylbenzenes, DABEs, respectively). We report the synthesis, anti-HIV activity and molecular modeling of 4,6-DAPY and DABE derivatives.

2. Results and discussion

2.1. Chemistry

Synthesis of 4,6-DAPYs. The synthesis of 4,6-diarylpyrimidine compounds is described in Scheme 1. The first step takes place by a Nucleophilic Aromatic Substitution (S_NAr) reaction between commercially available 4,6-dichloropyrimidine (**4**) and substituted phenols (**5a,b**) in dimethylformamide (DMF), K_2CO_3 and 18-crown-6 ether at 90 °C during 3 h, to provide **6a,b**, respectively. Then, compounds **6a,b** were coupled with different substituted anilines (**7a,b**) using palladium acetate as catalyst (Buchwald–Hartwig [18] reaction) to afford the corresponding target compounds **8a–d** (Scheme 1).

Synthesis of DABEs. These diarylbenzene derivatives were formed by different synthetic procedures depending on the linker moiety between the central ring and the wing I. For the compounds with an oxygen atom as linker group, the first step also involves a S_NAr reaction between the 3-fluoronitrobenzene (**9**) and 2,4,6-trimethylphenol (**10**) in DMF, K_2CO_3 and 18-crown-6 at 100 °C during 24 h to provide **11** (Scheme 2). Then, the nitro group of compound **11** was reduced to the amine leading to derivative **12**, which finally was coupled with substituted bromobenzenes (**13a,b**), according to Buchwald–Hartwig reaction, by the same

procedure described before, to obtain the desired diarylbenzenes, **14a,b** (Scheme 2).

When the linker moieties were only amine groups, the synthesis started with the S_NAr reaction between 1,3-diaminobenzene (**15**) and 4-fluorobenzonitrile (**16**) leading to the corresponding intermediate (**17**) using K_2CO_3 in DMF at 130 °C during 72 h. The next step was a Buchwald–Hartwig [18] reaction between **17** and 2,4,6-trimethylbromobenzene (**13a**), affording the diarylbenzene **18**, under the same condition as described above (Scheme 3).

Spectral data of all compounds are in full agreement with the proposed structures.

2.2. Biological activity

All 4,6-DAPY and DABE compounds were evaluated for antiviral activity and cytotoxicity using the MTT [(3-(4,5-dimethylthiazol-2-yl)-2,5-diphenyltetrazolium bromide)] method [19,20] in MT-4 cells infected with wild-type HIV-1 strain III_B, double mutant HIV-1 strain RES056 (K103N + Y181C) and HIV-2 strain ROD. Zidovudine (AZT), delavirdine (DEV), nevirapine (NVP) and etravirine (ETV), four drugs currently used in clinical treatment of HIV-1 infection, were also included as reference compounds. The biological evaluation is summarized in Table 1.

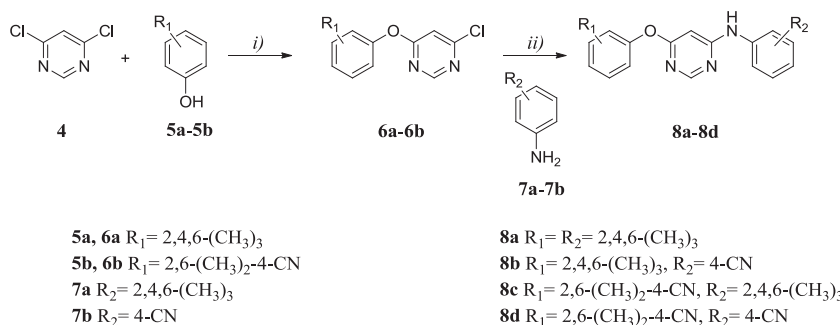
Except for compounds **8a** and **14a**, all the novel synthesized NNRTI exhibited from moderate (compound **8c**, $EC_{50} = 5.25 \mu M$) to excellent potency (compounds **8b**, **8d**, **14b** and **18**, EC_{50} from 0.049 to 0.599 μM) against wild-type virus. Of this series, compound **8b** was identified as the most active derivative against wild-type HIV-1 ($EC_{50} = 0.049 \mu M$ and selectivity index (SI) of 870).

Table 1 shows that derivatives **8d**, **14b** and **18** also displayed activity against wild-type HIV-1 at micromolar concentration level ($EC_{50} = 0.381$, 0.599 and 0.398 μM , respectively). Compound **8b** was 2-fold and 11-fold more potent than NEV and DEV against HIV-1 III_B strain, respectively. Meanwhile, compounds **8d** and **18**, were 1.5-fold more potent than DEV against the same strain. Unfortunately, the tested compounds were inactive against the double RT mutant (K103N + Y181C) HIV-1 RES056 strain and HIV-2 strain ROD.

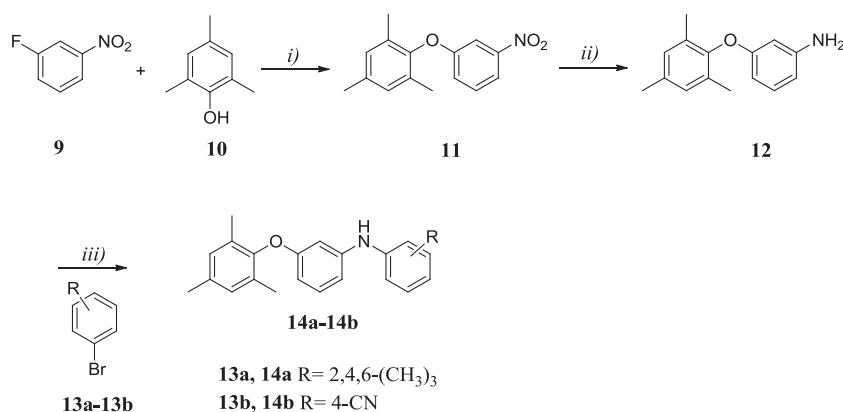
The molecular structure of the synthesized compounds shows that derivatives with a 2,4,6-trimethyl substituent in the wing II displayed moderate or no activity against the HIV-1 III_B strain (compounds **8a**, **14a** and **8c**); while compounds with a 4-nitrile substituent in the wing II exhibited an excellent potency against this strain.

2.3. Molecular modeling

Molecular docking was carried out for compounds **8a–d**; **14a,b** and **18** into the NNIBP of wtRT where these NNRTI are complexed (NNRTI-RT), using the software Autodock3 [21]. Then, NNRTI-RT



Scheme 1. Reagents and conditions: i) DMF, K_2CO_3 , 18-crown-6, 90 °C, 3 h; ii) $Pd(OAc)_2$, Xantphos, Cs_2CO_3 , xylene, 140 °C, 48 h.



Scheme 2. Reagents and conditions: i) DMF, K_2CO_3 , 18-crown-6, 100 °C, 24 h; ii) Pd/C 10%, H_2 , ethanol, 24 h; iii) Pd(OAc) $_2$, Xantphos, CS_2CO_3 , toluene, 100 °C, 48 h.

complexes were simulated by molecular dynamics (MD) and analyzed using Amber10 [22].

It is important to point out that the synthesized compounds adopted a very similar conformation of interaction in the NNBP to that of the reference DAPY compound **3**. These positions in the INNBP were maintained during the 3 ns MD simulations (Fig. 2). The novel NNRTIs accommodate wing I in the hydrophobic pocket lined by residues Pro95, Tyr181, Tyr188, Val189 and Trp229, and wing II in the pocket lined by Lys103, Val106, Gly190, Hie235, Pro236, Tyr318 (Figs. 2 and 3). The central ring established hydrophobic contacts with Leu100 and Glu138. Finally, some of the compounds undergo a hydrogen bond with residue Lys101 through the nitrogen atom of the central ring or the NH linker moiety with the wing II (Fig. 3).

The interaction between the Lys101 backbone carbonyl oxygen and the NH linker moiety present in the 4,6-DAPYs and DABEs compounds was followed during the 3 ns MD simulation (Table 2).

Compounds with excellent potency against wild-type virus (**8b**, **8d**, **14b** and **18**), showed sustained hydrogen bond interactions, with occupancies of 90.5, 91.9, 91.9 and 78.5%, respectively (Table 2). Compound **8c**, which has moderate antiviral potency, also established a hydrogen bond with a moderate occupancy of 61.1%. Finally, inactive derivatives **8a** and **14a**, had very low hydrogen bond occupancy with residue Lys101, of 29.0 and 14.6%, respectively. In addition, compounds **8b** and **8d** established hydrogen bond interactions with the NH moiety of residue Lys101 through the nitrogen atom of the 4,6-pyrimidine central ring, with occupancies of 10.6 and 17.2%, respectively. The highly potent reference compound ETV also showed high occupancy of this interaction (91.8%) [17]. Clearly, a critical feature for the inhibition of the wild-type strain of the enzyme is to establish and maintain hydrogen bond interaction with Lys101.

In order to analyze the position of wings I and II with respect to the central ring of the novel compounds, the dihedral angles τ_1 and τ_2 (Fig. 1) were studied during the MD trajectories (Table 2). In all cases, the dihedral angle τ_1 adopted a value closed to 90°, indicating that wing I is in a perpendicular position with respect to the

central ring. These results are in agreement with previous observations that methyl substitutions in the ortho positions of wing I favor this spatial arrangement due to steric hindrance, without restraining the flexibility of the ligand, and maximizing the π - π stacking interaction with Tyr181, Tyr188 and Trp229 [17].

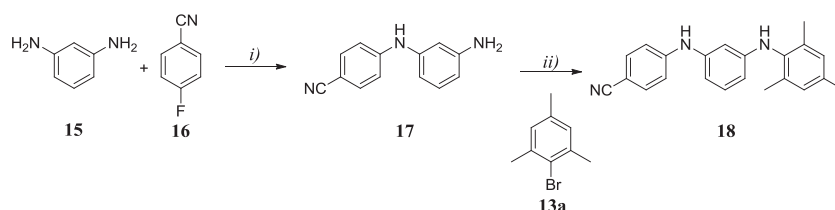
The antiviral molecules had different τ_2 values (Table 2). Derivatives with a nitrile substituent in the position 4 of the wing II (**8b**, **8d**, **14b**, **18** and ETV) adopted dihedral angles of less than 40°. The rest of the compounds (**8a**, **8c** and **14a**) adopted dihedral angles close to 90°, due to the presence of methyl substituents in positions 2, 4 and 6 in wing II. The trimethyl substitution in wing II forced the wing to adopt a perpendicular orientation respect to the central ring, similar to wing I, moving the inhibitor away from the Lys101 residue, and therefore breaking the biologically important hydrogen bond.

In order to prove this hypothesis, an electrostatic energy analysis between the novel compounds and the residue Lys101 was performed from the MD trajectories, using the Molecular Mechanics-Poisson Boltzmann Surface Area (MM-PBSA) approximation (Eq. (1), Experimental section). The compound with the highest antiviral activity (**8b**) maintained high electrostatic energy interaction with the residue Lys101, while the compound with the lowest activity (**8c**) showed the lowest electrostatic energy interaction (Table 3).

Fig. 4 shows the correlation between the electrostatic energy of interaction with Lys101 and the antiviral activity. Thus, the five active novel compounds present a significant dependency between these two parameters, showing the importance of the hydrogen bond interaction with Lys101 residue for the NNRTI, in order to produce an effective inhibition against the RT wild-type.

3. Conclusion

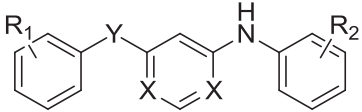
A series of novel NNRTIs scaffolds 4,6-DAPYs and DABEs were synthesized, evaluated for their activity against HIV and their interaction with RT was modeled. These novel compounds were designed based on conclusions from our previous molecular modeling studies of established NNRTI examples [17]. Among all tested derivatives, **8b** was identified as the most active compound



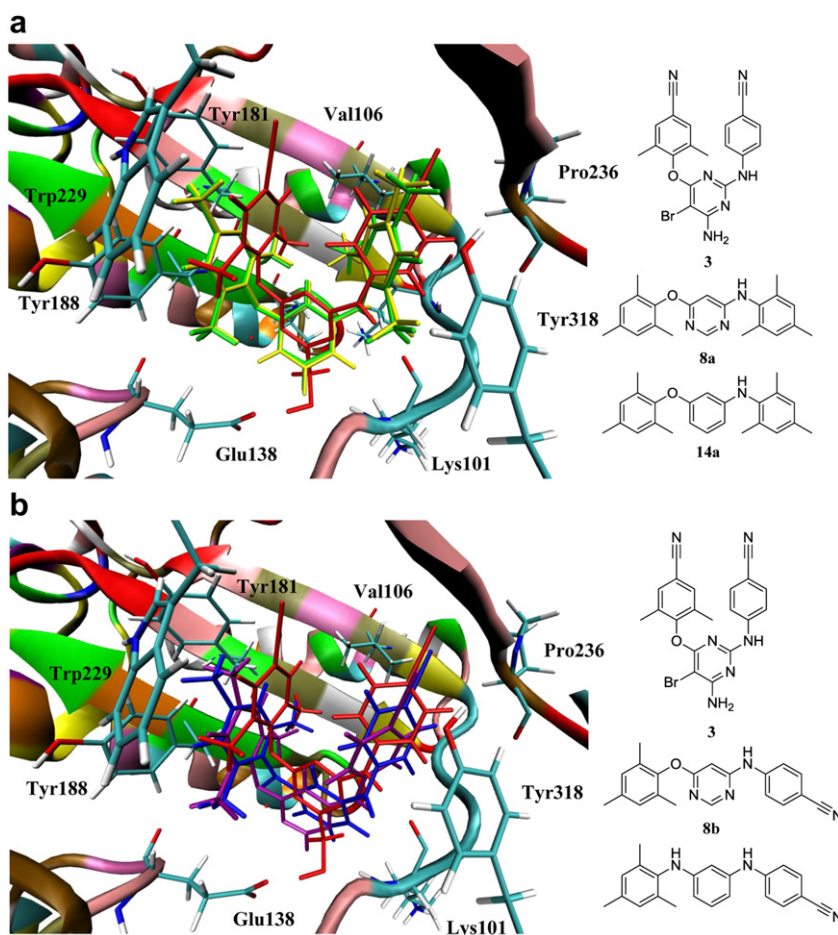
Scheme 3. Reagents and conditions: i) DMF, K_2CO_3 , 130 °C, 72 h; ii) Pd(OAc) $_2$, Xantphos, CS_2CO_3 , toluene, 100 °C, 48 h.

Table 1

Biological activities, cytotoxicities and selectivity indices of new designed 4,6-DAPY and DABE compounds.



	X	Y	R1	R2	EC ₅₀ ^a (μM)			CC ₅₀ ^b (μM)	SI ^c
					HIV-1		HIV-2		
					III _B ^d	RES056 ^e			
8a	N	O	2,4,6-(CH ₃) ₃	2,4,6-(CH ₃) ₃	>38.5	>38.5	>38.5	38.2 ± 2.82	<1
8b	N	O	2,4,6-(CH ₃) ₃	4-CN	0.049 ± 0.005	>42.21	>42.21	42.21 ± 8.91	870
8c	N	O	2,6-(CH ₃) ₂ -4-CN	2,4,6-(CH ₃) ₃	5.251 ± 0.363	>37.54	>37.54	37.54 ± 4.50	7
8d	N	O	2,6-(CH ₃) ₂ -4-CN	4-CN	0.381 ± 0.117	>291.8	>291.8	>291.8	≥740.1
14a	C	O	2,4,6-(CH ₃) ₃	2,4,6-(CH ₃) ₃	>43.62	>43.62	>43.62	43.62 ± 7.25	<1
14b	C	O	2,4,6-(CH ₃) ₃	4-CN	0.599 ± 0.330	>52.56	>52.56	52.56 ± 15.40	65
18	C	NH	2,4,6-(CH ₃) ₃	4-CN	0.398 ± 0.061	>220.18	>220.18	≥220.18	≥552
AZT					0.008 ± 0.002	0.006 ± 0.0004	0.006 ± 0.001	>93.63	>12,034
DEV					0.548 ± 0.285	>4.39	>4.39	>4.39	>8
NVP					0.097 ± 0.038	≥7.60	>14.99	>14.99	>155
ETV					0.002 ± 0.0004	0.034 ± 0.005	>27.79	27.79 ± 11.54	12,884

^a EC₅₀: effective concentration of compound required to protect the cell against viral cytopathogenicity by 50% in MT-4 cells.^b CC₅₀: cytotoxic concentration of compound that reduces the uninfected MT-4 cell viability by 50%.^c SI: selectivity index: ratio CC₅₀/EC₅₀.^d III_B: HIV-1 wild-type strain.^e RES056: HIV-1 mutated strain bearing both K103N and Y181C mutations.**Fig. 2.** Binding modes and superposition of compound **3** (red) in the crystallographic complex 1SUQ with a) molecular docking conformation of compound **8a** (green) and **14a** (yellow) and b) molecular docking conformation of compound **8b** (blue) and **18** (purple) to the NNIBP of wtRT. (For interpretation of the references to colour in this figure legend, the reader is referred to the web version of this article.)

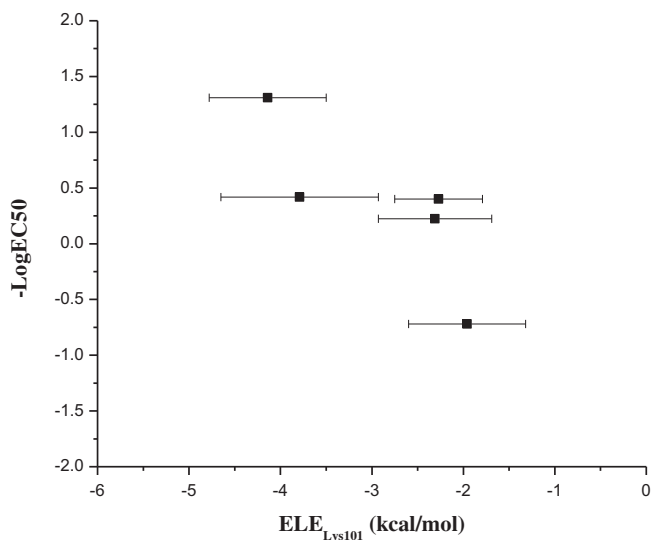


Fig. 4. Biological activity ($-\log EC_{50}$) vs. electrostatic energy interaction between residue Lys101 and the novel active compounds.

DMF were added to a dried flask of 50 mL and then, under continuing stirring, 18-crown-6 (0.25 mmol) was also added. The reaction mixture was heated to 90 °C under nitrogen atmosphere for 3 h. Next, the resulting reaction mixture was extracted with diethyl ether. The organic layer was dried over anhydrous sodium carbonate, filtered evaporated under reduced pressure and subsequently purified by medium pressure chromatography to give products **6a,b**.

4.1.1.1. 4-Chloro-6-(2,4,6-trimethylphenoxy)pyrimidine (**6a**). Yield 84%; white crystals; mp 64.4–66.9 °C; ^1H NMR (300 MHz, CDCl_3): δ 2.07 (s, 6H, CH_3 -7', CH_3 -8'), 2.31 (s, 3H, CH_3 -9'), 6.88 (s, 1H, CH -2), 6.93 (s, 2H, CH -3', 5'), 8.56 (s, 1H, CH -4); ^{13}C NMR (75 MHz, CDCl_3): δ 16.18, 20.76, 106.72, 129.57, 129.80, 135.85, 146.74, 158.82, 161.92, 169.77; HR-MS calcd. for $\text{C}_{13}\text{H}_{13}\text{ClN}_2\text{O}$ m/z 248.07164, found: 248.07268.

4.1.1.2. 4-Chloro-6-(4-cyano-2,6-dimethylphenoxy)pyrimidine (**6b**). Yield 80%; white crystals; mp: 135.2–139.1 °C; ^1H NMR (300 MHz, CDCl_3): δ 2.14 (s, 6H, CH_3 -7', 8'), 7.06 (s, 1H, CH -2), 7.45 (s, 2H, CH -3', 5'), 8.52 (s, 1H, CH -4); ^{13}C NMR (75 MHz, CDCl_3): δ 16.49, 107.49, 110.41, 118.48, 132.61, 132.85, 152.75, 158.80, 162.58, 168.81; HR-MS calcd. for $\text{C}_{13}\text{H}_{10}\text{ClN}_3\text{O}$ m/z 259.05124, found: 259.05119.

4.1.2. General procedure for the preparation of **8a–d**

In a dried screw tube of 10 mL, 4-chloropyrimidine (**6a,b**) (0.5 mmol), substituted anilines (**7a,b**) (0.6 mmol), $\text{Pd}(\text{OAc})_2$ (0.025 mmol), Xantphos (0.05 mmol), Cs_2CO_3 (1.0 mmol) and xylene (5 mL) were added, under nitrogen atmosphere and continuous stirring at 100–140 °C until the chloropyrimidine was consumed. The course of the reaction was followed by thin layer chromatography (TLC) analysis. Next, the resulting reaction was extracted with diethyl ether, dried over anhydrous sodium carbonate, filtered and purified by medium pressure chromatography to give products **8a–d**.

4.1.2.1. 6-(2,4,6-Trimethylaniline)-4-(2,4,6-trimethylphenoxy)pyrimidine (**8a**). Yield 29%; yellow solid; ^1H NMR (300 MHz, CDCl_3): δ 2.04 (s, 6H, CH_3 -8', CH_3 -9'), 2.20 (s, 6H, CH_3 -7'', CH_3 -8''), 2.26 (s, 3H, CH_3 -10'), 2.31 (s, 3H, CH_3 -9''), 5.43 (s, 1H, NH -7'), 6.73 (s, 1H, CH -2), 6.86 (s, 2H, CH -3', CH -5'), 6.96 (s, 2H, CH -3'', CH -5''), 8.23 (s, 1H, CH -4). ^{13}C NMR (75 MHz, CDCl_3): δ 16.45, 18.27, 20.95, 21.08,

84.79, 129.38, 129.51, 130.42, 131.79, 135.06, 136.38, 137.53, 147.52, 158.77, 164.43, 170.11; HR-MS calcd. for $\text{C}_{22}\text{H}_{25}\text{N}_3\text{O}$ m/z 347.19976, found: 337.19973.

4.1.2.2. 4-[4-(2,4,6-Trimethylphenoxy)pyrimidin-6-ylamino]benzotrile (**8b**). Yield 89%; yellow solid; mp 197.5–201.7 °C; ^1H NMR (300 MHz, CDCl_3): δ 2.09 (s, 6H, CH_3 -7'', CH_3 -8''), 2.29 (s, 3H, CH_3 -9''), 6.19 (s, 1H, NH -7'), 6.91 (s, 2H, CH -3'', CH -5''), 7.26 (s, 1H, CH -2), 7.58 (d, $J = 8.7$ Hz, 2H, CH -2', CH -6'), 7.63 (d, $J = 8.7$ Hz, 2H, CH -3', CH -5'), 8.44 (s, 1H, CH -4); ^{13}C NMR (75 MHz, CDCl_3): δ 16.47, 21.00, 88.75, 106.22, 119.10, 119.95, 129.69, 130.35, 133.63, 135.67, 143.19, 147.24, 159.06, 161.62, 170.13; HR-MS calcd. for $\text{C}_{20}\text{H}_{18}\text{N}_4\text{O}$ m/z 330.14806, found: 330.14792.

4.1.2.3. 2,6-Dimethyl-4-[4-(2,4,6-trimethylaniline)pyrimidin-6-yloxy]benzotrile (**8c**). Yield 21%; white solid; mp: 166.0–168.5 °C; ^1H NMR (300 MHz, CDCl_3): δ 2.11 (s, 6H, CH_3 -8', CH_3 -9'), 2.22 (s, 6H, CH_3 -7'', CH_3 -8''), 2.33 (s, 3H, CH_3 -10'), 5.49 (s, 1H, NH -7'), 6.79 (s, 1H, CH -2), 6.99 (s, 2H, CH -3', CH -5'), 7.38 (s, 2H, CH -3'', CH -5''), 8.19 (s, 1H, CH -4). ^{13}C NMR (75 MHz, CDCl_3): δ 16.53, 18.28, 21.13, 84.93, 109.50, 118.89, 129.65, 131.45, 132.58, 132.96, 136.36, 137.89, 153.63, 158.61, 164.67, 169.19; HR-MS calcd. for $\text{C}_{20}\text{H}_{18}\text{N}_4\text{O}$ m/z 358.17936, found: 358.17954.

4.1.2.4. 4-[4-(4-Cyano-2,6-dimethylphenoxy)pyrimidin-6-ylamino]benzotrile (**8d**). Yield 24%; white solid; mp: 198.9–200.7 °C; ^1H NMR (300 MHz, CDCl_3): δ 2.16 (s, 6H, CH_3 -7'', CH_3 -8''), 6.36 (s, 1H, NH -7'), 7.18 (s, 1H, CH -2), 7.43 (s, 2H, CH -3'', CH -5''), 7.61 (d, $J = 8.4$ Hz, 2H, CH -2', CH -6'), 7.67 (d, $J = 8.4$ Hz, 2H, CH -3', CH -5'), 8.38 (s, 1H, CH -4); ^{13}C NMR (75 MHz, CDCl_3): δ 16.58, 89.06, 106.68, 109.90, 118.73, 118.97, 120.27, 132.76, 132.94, 133.70, 142.88, 153.30, 158.87, 161.84, 169.02; HR-MS calcd. for $\text{C}_{20}\text{H}_{15}\text{N}_5\text{O}$ m/z 341.12766, found: 341.12893.

4.1.3. 3-(2,4,6-Trimethylphenoxy)-1-nitrobenzene (**11**)

To a dried flask of 50 mL, 2,4,6-trimethylphenol (**10**) (10 mmol), potassium carbonate (20 mmol) and 20 mL of DMF were added. Then, 3-fluoro-1-nitrobenzene (**9**) (10 mmol) was added to the flask via a syringe, followed by 18-crown-6 (0.5 mmol) in continuing stirring. The reaction was heated at 90 °C under nitrogen atmosphere during 24 h. Next, the resulting reaction was extracted with diethyl ether. The organic layer was dried over anhydrous sodium carbonate, filtered and evaporated under reduced pressure before purification by medium pressure chromatography to obtain **11**. Yield 54%; orange solid; mp: 65.3–70.5 °C; ^1H NMR (300 MHz, CDCl_3): δ 2.07 (s, 6H, CH_3 -7', CH_3 -8'), 2.31 (s, 3H, CH_3 -9'), 6.93 (s, 2H, CH -3', CH -5'), 7.12 (d, $J = 8.1$ Hz, 1H, CH -6), 7.41 (t, $J = 8.1$ Hz, 1H, CH -5), 7.56 (s, 1H, CH -2), 7.83 (d, $J = 7.8$, 1H, CH -4); ^{13}C NMR (75 MHz, CDCl_3): δ 16.28, 20.92, 109.71, 116.42, 121.14, 130.10, 130.37, 130.62, 135.51, 148.11, 149.61, 158.82; HR-MS calcd. for $\text{C}_{15}\text{H}_{15}\text{NO}_3$ m/z 257.10519, found: 257.10419.

4.1.4. 3-(2,4,6-Trimethylphenoxy)aniline (**12**)

To a dried flask of 50 mL, compound **11** (2.1 mmol), 21 mg of Pd/C 10% and 20 mL of ethanol were added under hydrogen atmosphere at room temperature during 24 h. After this time, the resulting reaction was extracted with diethyl ether, and the organic layer was dried over anhydrous sodium carbonate, filtered and purified by medium pressure chromatography to obtain **12**. Yield 93%, uncolored oil; ^1H NMR (300 MHz, CDCl_3): δ 2.09 (s, 6H, CH_3 -7', CH_3 -8'), 2.29 (s, 3H, CH_3 -9'), 3.59 (s, 2H, NH -7), 6.08 (s, 1H, CH -2), 6.16 (d, $J = 8.1$ Hz, 1H, CH -6), 6.27 (d, $J = 7.8$ Hz, 1H, CH -4), 6.88 (s, 2H, CH -3', CH -5'), 6.99 (t, $J = 7.8$ Hz, 1H, CH -5). ^{13}C NMR (75 MHz, CDCl_3): δ 16.38, 20.92, 101.53, 105.23, 108.37, 129.56, 130.34, 131.27, 134.38, 148.00, 148.98, 159.34; HR-MS calcd. for $\text{C}_{15}\text{H}_{15}\text{NO}_3$ m/z 227.13101, found: 227.12980.

4.1.5. General procedure for the preparation of **14a,b**

In a dried screw tube, **12** (0.6 mmol), bromobenzene compounds (**13a** or **13b**) (0.4 mmol), Pd(AcO)₂ (0.03 mmol), Xantphos (0.06 mmol), Cs₂CO₃ (0.8 mmol) and toluene (5 mL) were added under nitrogen atmosphere and heated with stirring to 100 °C until the bromide compound disappeared, which was monitored by TLC analysis. Next, the resulting reaction mixture was extracted with diethyl ether, dried over anhydrous sodium carbonate, filtered and purified by medium pressure chromatography to obtain **14a,b**.

4.1.5.1. *N*-[3-(2,4,6-Trimethylphenoxy)phenyl]-*N*-(2,4,6-trimethylphenyl)amine (**14a**). Yield 27%; white solid, mp: 122.2–124.1 °C; ¹H NMR (300 MHz, CDCl₃): δ 2.09 (s, 6H, CH₃-8', CH₃-9'), 2.16 (s, 6H, CH₃-7'', CH₃-8''), 2.28 (s, 3H, CH₃-10'), 2.29 (s, 3H, CH₃-9''), 5.04 (s, 1H, NH-7'), 6.01 (d, *J* = 9.0 Hz, 1H, CH-4), 6.02 (s, 1H, CH-2), 6.04 (d, *J* = 9.0 Hz, 1H, CH-6), 6.87 (s, 2H, CH-3', CH-5'), 6.91 (s, 2H, CH-3'', CH-5''), 6.93 (t, *J* = 7.8 Hz, 1H, CH-5). ¹³C NMR (75 MHz, CDCl₃): δ 16.42, 18.36, 20.91, 21.02, 100.39, 104.10, 106.58, 129.31, 129.52, 130.05, 131.28, 134.25, 135.57, 135.58, 136.11, 148.48, 149.20, 159.52; HR-MS calcd. for C₂₄H₂₇NO *m/z* 345.20926, found: 345.20968.

4.1.5.2. 4-[3-(2,4,6-Trimethylphenoxy)phenyl-1-ylamino]benzotrile (**14b**). Yield 49%; white solid; mp: 162.0–163.5 °C; ¹H NMR (300 MHz, CDCl₃): δ 2.10 (s, 6H, CH₃-7'', CH₃-8''), 2.29 (s, 3H, CH₃-9''), 6.05 (s, 1H, NH-7'), 6.49 (d, *J* = 8.4 Hz, 1H, CH-4), 6.54 (s, 1H, CH-2), 6.78 (d, *J* = 8.4 Hz, 1H, CH-6), 6.90 (s, 2H, CH-3'', CH-5''), 6.96 (d, *J* = 8.8 Hz, 2H, CH-2', CH-6'), 7.19 (t, *J* = 8.0 Hz, 1H, CH-5), 7.46 (d, *J* = 8.8 Hz, 2H, CH-3', CH-5'). ¹³C NMR (75 MHz, CDCl₃): δ 16.35, 20.90, 101.93, 107.15, 110.19, 113.46, 115.40, 119.93, 129.76, 130.63, 131.00, 133.84, 134.81, 141.65, 147.70, 148.73, 159.42; HR-MS calcd. for C₂₂H₂₀N₂O *m/z* 328.15756, found: 328.15643.

4.1.6. 4-(3-Aminophenyl-1-yl-amino)benzotrile (**17**)

Potassium carbonate (40 mmol), 1,3-diaminobenzene (**15**) (30 mmol) and 4-fluorobenzotrile (**16**) (20 mmol) were added to a dried flask with 50 mL of anhydrous DMF. The reaction mixture was heated to 130 °C under nitrogen atmosphere and continuing stirring for 72 h. The resulting reaction mixture was extracted with diethyl ether. The organic layer was dried over anhydrous sodium carbonate, filtered and purified by medium pressure chromatography to obtain **17**. Yield 5.0%; brown solid; mp: 150.9–153.8 °C; ¹H NMR (300 MHz, CDCl₃): δ 3.70 (s, 2H, NH-7), 5.95 (s, 1H, NH-7'), 6.41 (d, *J* = 7.8 Hz, 1H, CH-4), 6.46 (s, 1H, CH-2), 6.51 (d, *J* = 7.8 Hz, 1H, CH-6), 6.94 (d, *J* = 8.7 Hz, 2H, CH-2', CH-6'), 7.09 (t, *J* = 7.8 Hz, 1H, CH-5), 7.44 (d, *J* = 8.7 Hz, 2H, CH-3', CH-5'). ¹³C NMR (75 MHz, CDCl₃): δ 101.49, 107.50, 110.97, 111.43, 115.33, 120.08, 130.60, 133.84, 141.19, 147.84, 148.12.

4.1.7. 4-[3-(2,4,6-Trimethylaniline)phenyl-1-ylamino]benzotrile (**18**)

To a dried screw tube of 10 mL, **17** (0.6 mmol), 2,4,6-trimethylbromobenzene (**13a**) (0.5 mmol), Pd(OAc)₂ (0.025 mmol), Xantphos (0.05 mmol), Cs₂CO₃ (1.0 mmol) and toluene (5 mL) were added. Then, the reaction mixture was stirred under nitrogen atmosphere at 100 °C, until the brominated compound was consumed, which was monitored by TLC analysis. Then, the resulting reaction mixture was extracted with diethyl ether. The organic layer was dried over anhydrous sodium carbonate, filtered, evaporated under reduced pressure and purified by medium pressure chromatography to obtain **18**. Yield 75.8%; white solid, mp: 218.6–222.4 °C; ¹H NMR (300 MHz, CDCl₃): δ 2.19 (s, 6H, CH₃-8'', CH₃-10''), 2.30 (s, 3H, CH₃-9''), 5.13 (s, 1H, NH-7'), 5.90 (s, 1H, NH-7''), 6.15 (s, 1H, CH-2), 6.30 (d, *J* = 7.8 Hz, 1H, CH-4), 6.55 (d, *J* = 7.8 Hz, 1H, CH-6), 6.93 (d, *J* = 8.7 Hz, 2H, CH-2', CH-6'), 6.94 (s, 2H, CH-3'', CH-5''), 7.11 (t, *J* = 7.8 Hz, 1H, CH-5), 7.44 (d, *J* = 8.7 Hz, 2H, CH-3', CH-5'). ¹³C NMR

(75 MHz, CDCl₃): δ 18.16, 20.87, 101.11, 105.16, 109.26, 110.27, 114.97, 119.92, 129.22, 130.21, 133.59, 134.91, 135.87, 136.09, 141.01, 147.96, 148.15; HR-MS calcd. for C₂₂H₂₁N₃ *m/z* 327.17355, found: 327.17333.

4.2. Anti-HIV activity assay

The anti-HIV activity and cytotoxicity of the compounds **8a–d**, **14a,b** and **18** were evaluated against wild-type HIV-1 strain III_B, a double RT mutant (K103N + Y181C) HIV-1 strain and HIV-2 strain ROD in MT-4 cell cultures using the 3-(4,5-dimethylthiazol-2-yl)-2,5-diphenyltetrazoliumbromide (MTT) method [19,20]. Briefly, stock solutions (10× final concentration) of test compounds were added in 25 μL volumes to two series of triplicate wells so as to allow simultaneous evaluation of their effects on mock- and HIV-infected cells at the beginning of each experiment. Serial 5-fold dilutions of test compounds were made directly in flat-bottomed 96-well microtiter trays using a Biomek 3000 robot (Beckman instruments). Untreated control HIV- and mock-infected cell samples were included for each sample. Virus stock (50 μL) at 100–300 CCID₅₀ (50% cell culture infectious dose) or culture medium was added to either the virus-infected or mock-infected wells of the microtiter tray. Mock-infected cells were used to evaluate the effect of test compounds on uninfected cells in order to assess the cytotoxicity of the test compounds. Exponentially growing MT-4 cells were centrifuged for 5 min at 220 g and the supernatant was discarded. The MT-4 cells were resuspended at 6 × 10⁵ cells/mL and 50 μL volumes were transferred to the microtiter tray wells. Five days after infection, the viability of mock- and HIV-infected cells was examined spectrophotometrically by the MTT assay.

The MTT assay is based on the reduction of yellow colored MTT (Acros Organics) by mitochondrial dehydrogenase activity of metabolically active cells to a blue-purple formazan that can be measured spectrophotometrically. The absorbances were read in an eight-channel computer-controlled photometer (Infinite M1000, Tecan), at two wavelengths (540 and 690 nm). All data were calculated using the median OD (optical density) values of tree wells. The 50% cytotoxic concentration (CC₅₀) was defined as the concentration of the test compound that reduced the absorbance (OD₅₄₀) of the mock-infected control sample by 50%. The concentration achieving 50% protection from the cytopathic effect of the virus in infected cells was defined as the 50% effective concentration (EC₅₀).

4.3. Molecular modeling

The novel NNRTIs were built using the Gabedit software [23], after which conformational searches were performed using Gaussian03 [24], applying the AM1 semi-empirical method [25]. The minimum energy conformation was further optimized at the *ab-initio* (HF6-31G*) level, with the goal of obtaining a minimum energy conformation that allowed a representative charge assignment over each atom. In this way, restrained electrostatic potential (RESP) fitted charges were computed using Gaussian03. Atom parameters are added using the ff99 force field with the module xLeap of Amber10 [22].

As in previous work [17], the crystallographic structure of the wtRT in complex with the reference compound **3** (PDB ID: 1SUQ [26]) was used to performed all the molecular modeling analysis. First, the crystallographic structure was subjected to energy minimization with the sander module of Amber10 [22]. Affinity grids were constructed on the minimized structures using AutoGrid [27]. Docking assays were carried out using the AutodockTools and Autodock3 [21]. The lowest-energy and most populated clusters of docked conformations were selected for the MD simulations. Intermolecular interactions were visualized with LigPlot [28].

The wtRT-NNRTI complexes were solvated using a pre-equilibrated TIP3P water model, applying a solvent box with a minimum distance from the solute of 8 Å in each direction. After minimization and equilibration, MDs were carried out at 300 K for 3 ns, using the *pmemd* module of Amber10 [22]. Hydrogen bonds and dihedral angles analyses were studied with the *ptraj* module of Amber10 [22]. The trajectories were processed using VMD software [29]. The electrostatic energy component analysis was estimated by the Molecular Mechanics-Poisson Boltzmann Surface Area (MM-PBSA) method [30], integrated in Amber10 [22]:

$$G = E_{MM} + G_{solv} - T\Delta S \quad (1)$$

where, G is the Gibbs free energy, T is the absolute temperature, ΔS is the entropic changes, E_{MM} is the total molecular mechanic energy, which includes internal (bond, angle, dihedral), van der Waals and electrostatic terms; $G_{solv} = G_{pol} + G_{np}$; G_{pol} is the electrostatic component of the solvation free energy, which was computed by the Poisson-Boltzmann approximation [31]; and G_{np} is the non-polar contribution to the solvation free energy, calculated by an empirical model. The solvent was treated as a continuum model of high-dielectric ($\epsilon = 80$) and the solute as a low-dielectric media ($\epsilon = 1$) with embedded charges [32].

Acknowledgments

The authors gratefully acknowledge financial support from the Secretaría de Ciencia y Técnica of the Universidad Nacional de Córdoba (SECYT-UNC) and the Ministerio de Ciencia y Tecnología (MINCYT) of Córdoba, as well as the Consejo Nacional de Investigaciones Científicas y Técnicas (CONICET), the Agencia Nacional de Promoción Científica y Tecnológica (FONCYT) of Argentina and grant GOA 10/14 from KU Leuven. This research was supported in part by the National Science Foundation through XSEDE resources provided by the Pittsburgh Supercomputing Center (TG-MCB070064). Sergio R. Ribone also acknowledges fellowships from CONICET and Erasmus Mundus External Cooperation Windows (EADIC Lot 16).

Appendix A. Supplementary data

Supplementary data related to this article can be found at <http://dx.doi.org/10.1016/j.ejmech.2012.10.036>.

References

- [1] F.J. Palella Jr., R.K. Baker, A.C. Moorman, J.S. Chmiel, K.C. Wood, J.T. Brooks, S.D. Holmberg, Mortality in the highly active antiretroviral therapy era: changing causes of death and disease in the HIV outpatient study, *J. Acquir. Immune Defic. Syndr.* 43 (2006) 27.
- [2] Y. Mehellou, E. De Clercq, Twenty-six years of anti-HIV drug discovery: where do we stand and where do we go? *J. Med. Chem.* 53 (2010) 521.
- [3] X. Chen, P. Zhan, D. Li, E. De Clercq, X. Liu, Recent advances in DAPYs and related analogues as HIV-1 NNRTIs, *Curr. Med. Chem.* 18 (2011) 359.
- [4] M.P. de Béthune, Non-nucleoside reverse transcriptase inhibitors (NNRTIs), their discovery, development, and use in the treatment of HIV-1 infection: a review of the last 20 years (1989–2009), *Antiviral. Res.* 85 (2010) 75.
- [5] P. Zhan, X. Liu, *Expert Opin. Ther. Pat.* 21 (2011) 717.
- [6] E. De Clercq, Non-nucleoside reverse transcriptase inhibitors (NNRTIs), *Expert Opin. Investig. Drugs* 3 (1994) 253.
- [7] J. Ding, K. Das, C. Tantillo, W. Zhang, A.D. Clark Jr., S. Jessen, X. Lu, Y. Hsiou, A. Jacobo-Molina, K. Andries, R. Pauwels, H. Moereels, L. Koymans, P.A.J. Janssen, R.H. Smith Jr., M. Kroeger Koepke, C.J. Michejda, S.H. Hughes, E. Arnold, Structure of HIV-1 reverse transcriptase in a complex with the non-nucleoside inhibitor α -APA R 95845 at 2.8 Å resolution, *Structure* 3 (1995) 365.
- [8] P.G. Wyatt, R.C. Bethell, N. Cammack, D. Charon, N. Dodic, B. Dumaitre, D.N. Evans, D.V.S. Green, P.L. Hopewell, D.C. Humber, *J. Med. Chem.* 38 (1995).
- [9] J.H. Chan, G.A. Freeman, J.H. Tidwell, K.R. Romines, L.T. Schaller, J.R. Cowan, S.S. Gonzales, C.W. Lowell, C. Andrews III, D.J. Reynolds, M. St. Clair, R.J. Hazen, R.G. Ferris, K.L. Creech, G.B. Roberts, S.A. Short, K. Weaver, G.W. Koszalka, L.R. Boone, *J. Med. Chem.* 47 (2004) 1175.
- [10] A. Mai, M. Artico, G. Sbardella, S. Massa, E. Novellino, G. Greco, A.G. Loi, E. Tramontano, M.E. Marongiu, P. La Colla, *J. Med. Chem.* 42 (1999) 619.
- [11] Y.-P. Wang, F.-E. Chen, J. Balzarini, E. De Clercq, C. Pannecouque, *Chem. Bio-divers.* 5 (2008) 168.
- [12] D.W. Ludovici, R.W. Kavash, M.J. Kukla, C.Y. Ho, H. Ye, B.L. De Corte, K. Andries, M.P. De Béthune, H. Azijn, R. Pauwels, H.E.L. Moereels, J. Heeres, L.M.H. Koymans, M.R. De Jonge, K.J.A. Van Aken, F.F.D. Daeyaert, P.J. Lewi, K. Das, E. Arnold, P.A.J. Janssen, Evolution of anti-HIV drug candidates. Part 2: diaryl-triazine (DATA) analogues, *Bioorg. Med. Chem. Lett.* 11 (2001) 2229–2234.
- [13] Y.-Z. Xiong, F.-E. Chen, J. Balzarini, E. De Clercq, C. Pannecouque, *Eur. J. Med. Chem.* 43 (2008) 1230.
- [14] D.W. Ludovici, B.L. De Corte, M.J. Kukla, H. Ye, C.Y. Ho, M.A. Lichtenstein, R.W. Kavash, K. Andries, M.P. De Béthune, H. Azijn, R. Pauwels, P.J. Lewi, J. Heeres, L.M.H. Koymans, M.R. De Jonge, K.J.A. Van Aken, F.F.D. Daeyaert, K. Das, E. Arnold, P.A.J. Janssen, Evolution of anti-HIV drug candidates. Part 3: diaryl-pyrimidine (DAPY) analogues, *Bioorg. Med. Chem. Lett.* 11 (2001) 2235–2239.
- [15] Y.-H. Liang, Q.-Q. He, Z.-S. Zeng, Z.-Q. Liu, X.-Q. Feng, F.-E. Chen, J. Balzarini, C. Pannecouque, E. De Clercq, *Bioorg. Med. Chem.* 18 (2010) 4601.
- [16] X.-Q. Zeng, Z.-S. Zeng, Y.-H. Liang, F.-E. Chen, C. Pannecouque, J. Balzarini, E. De Clercq, *Bioorg. Med. Chem.* 18 (2010) 2370.
- [17] S.R. Ribone, M.A. Quevedo, M. Madrid, M.C. Briñón, Rational approaches for the design of effective human immunodeficiency virus type 1 nonnucleoside reverse transcriptase inhibitors, *J. Chem. Inf. Model.* 51 (2011) 130.
- [18] S.L. Buchwald, L. Jiang, Palladium-catalyzed aromatic carbon–nitrogen bond formation, in: A. de Meijere, F. Diederich (Eds.), *Metal-Catalyzed Cross-Coupling Reactions*, Wiley-VCH, 2004, pp. 699–760.
- [19] C. Pannecouque, D. Daelemans, E. De Clercq, Tetrazolium-based colorimetric assay for the detection of HIV replication inhibitors: revisited 20 years later, *Nat. Protoc.* 3 (2008) 427–434.
- [20] R. Pauwels, J. Balzarini, M. Baba, R. Snoeck, D. Schols, P. Herdewijn, J. Desmyter, E. De Clercq, Rapid and automated tetrazolium-based colorimetric assay for the detection of anti-HIV compounds, *J. Virol. Methods* 20 (1988) 309–321.
- [21] G.M. Morris, D.S. Goodsell, R. Huey, W.E. Hart, S. Halliday, R. Belew, A.J. Olson, Autodock3.0, in: *Molecular Graphics Laboratory*, Department of Molecular Biology, The Scripps Research Institute, 1999.
- [22] D.A. Case, T.A. Darden, T.E. Cheatham, C.L. Simmerling, J. Wang, R.E. Duke, R. Luo, M. Crowley, W. Walker, K.M. Zhang, K.M. Merz, B. Wang, S. Hayik, A. Roitberg, G. Seabra, I. Kolossvary, K.F. Wong, F. Paesani, J. Vanicek, X. Wu, S.R. Brozell, T. Steinbrecher, H. Gohlke, L. Yang, C. Tan, J. Mongan, V. Hornak, G. Cui, D.H. Matthews, M.G. Seetin, C. Sagui, V. Babin, P.A. Kollman, AMBER10, University of California, San Francisco, 2008.
- [23] A.R. Allouche, Gabedit – a graphical user interface for computational chemistry softwares, *J. Comput. Chem.* 32 (2011) 174–182.
- [24] M.J. Frisch, G.W. Trucks, H.B. Schlegel, G.E. Scuseria, M.A. Robb, J.R. Cheeseman, J. Montgomery, J.A., T. Vreven, K.N. Kudin, J.C. Burant, J.M. Millam, S.S. Iyengar, J. Tomasi, V. Barone, B. Mennucci, M. Cossi, G. Scalmani, N. Rega, G.A. Petersson, H. Nakatsuji, M. Hada, M. Ehara, K. Toyota, R. Fukuda, J. Hasegawa, M. Ishida, T. Nakajima, Y. Honda, O. Kitao, H. Nakai, M. Klene, X. Li, J.E. Knox, H.P. Hratchian, J.B. Cross, V. Bakken, C. Adamo, J. Jaramillo, R. Gomperts, R.E. Stratmann, O. Yazyev, A.J. Austin, R. Cammi, C. Pomelli, J.W. Ochterski, P.Y. Ayala, K. Morokuma, G.A. Voth, P. Salvador, J.J. Dannenberg, V.G. Zakrzewski, S. Dapprich, A.D. Daniels, M.C. Strain, O. Farkas, D.K. Malick, A.D. Rabuck, K. Raghavachari, J.B. Foresman, J.V. Ortiz, Q. Cui, A.G. Baboul, S. Clifford, J. Cioslowski, B.B. Stefanov, G. Liu, A. Liashenko, P. Piskorz, I. Komaromi, R.L. Martin, D.J. Fox, T. Keith, M.A. Al-Laham, C.Y. Peng, A. Nanayakkara, M. Challacombe, P.M.W. Gill, B. Johnson, W. Chen, M.W. Wong, C. Gonzalez, J.A. Pople, Gaussian03, Gaussian Inc., Wallingford CT, 2004.
- [25] M.J.S. Dewar, E.G. Zoebisch, E.F. Healy, J.J.P. Stewart, AM1: a new general purpose quantum mechanical molecular model, *J. Am. Chem. Soc.* 107 (1985) 3902–3909.
- [26] K. Das, A.D. Clark Jr., P.J. Lewi, J. Heeres, M.R. De Jonge, L.M.H. Koymans, H.M. Vinkers, F. Daeyaert, D.W. Ludovici, M.J. Kukla, B. De Corte, R.W. Kavash, C.Y. Ho, H. Ye, M.A. Lichtenstein, K. Andries, R. Pauwels, M.P. De Béthune, P.L. Boyer, P. Clark, S.H. Hughes, P.A.J. Janssen, E. Arnold, Roles of conformational and positional adaptability in structure-based design of TMC125-R165335 (Etravirine) and related non-nucleoside reverse transcriptase inhibitors that are highly potent and effective against wild-type and drug-resistant HIV-1 variants, *J. Med. Chem.* 47 (2004) 2550–2560.
- [27] G.M. Morris, D.S. Goodsell, S. Halliday, R. Huey, W.E. Hart, R. Belew, A.J. Olson, Automated docking using a Lamarckian genetic algorithm and an empirical binding free energy function, *J. Comput. Chem.* 19 (1998) 1639–1662.
- [28] A.C. Wallace, R.A. Laskowski, J.M. Thornton, LIGPLOT: a program to generate schematic diagrams of protein-ligand interactions, *Protein Eng.* 8 (1995) 127.
- [29] W. Humphrey, A. Dalke, K. Schulten, VMD: visual molecular dynamics, *J. Mol. Graphics* 14 (1996) 33–38.
- [30] B. Kuhn, P. Gerber, T. Schulz-Gasch, M. Stahl, Validation and use of the MM-PBSA approach for drug discovery, *J. Med. Chem.* 48 (2005) 4040–4048.
- [31] K.A. Sharp, B. Honing, Electrostatic interactions in macromolecules: theory and applications, *Annu. Rev. Biophys. Biophys. Chem.* 19 (1990) 301–332.
- [32] W.D. Cornell, P. Cieplak, C.I. Bayly, I.R. Cough, K.M. Merz, D.M. Ferguson, D.C. Spellmeyer, T. Fox, J.W. Caldwell, P.A. Kollman, A second generation force field for the simulation of proteins, nucleic acids, and organic molecules, *J. Am. Chem. Soc.* 117 (1995) 5179–5197.